Deep–Sea Research I 186 (2022) 103824

Contents lists available at ScienceDirect

Deep-Sea Research Part I

journal homepage: www.elsevier.com/locate/dsri

# Water mass transformation in the Iceland Sea: Contrasting two winters separated by four decades

Kjetil Våge [a,*], Stefanie Semper [a,b], Héðinn Valdimarsson [c], Steingrímur Jónsson [d,c], Robert S. Pickart [b], G.W.K. Moore [e]

[a] Geophysical Institute, University of Bergen and Bjerknes Centre for Climate Research, Bergen, Norway
[b] Woods Hole Oceanographic Institution, Woods Hole, USA
[c] Marine and Freshwater Research Institute, Reykjavik, Iceland
[d] University of Akureyri, Akureyri, Iceland
[e] University of Toronto, Toronto, Canada

ARTICLE INFO

*Keywords:*
Iceland Sea
Water mass transformation
North Icelandic Jet
Iceland–Faroe Slope Jet
East Greenland Current
Denmark Strait overflow water

ABSTRACT

Dense water masses formed in the Nordic Seas flow across the Greenland–Scotland Ridge and contribute substantially to the lower limb of the Atlantic Meridional Overturning Circulation. Originally considered an important source of dense water, the Iceland Sea gained renewed interest when the North Icelandic Jet — a current transporting dense water from the Iceland Sea into Denmark Strait — was discovered in the early 2000s. Here we use recent hydrographic data to quantify water mass transformation in the Iceland Sea and contrast the present conditions with measurements from hydrographic surveys conducted four decades earlier. We demonstrate that the large-scale hydrographic structure of the central Iceland Sea has changed significantly over this period and that the locally transformed water has become less dense, in concert with a retreating sea-ice edge and diminished ocean-to-atmosphere heat fluxes. This has reduced the available supply of dense water to the North Icelandic Jet, but also permitted densification of the East Greenland Current during its transit through the presently ice-free western Iceland Sea in winter. Together, these changes have significantly altered the contribution from the Iceland Sea to the overturning in the Nordic Seas over the four decade period.

## 1. Introduction

As part of the large-scale overturning in the Atlantic Ocean, warm water flows northward and cold, densified water returns to the south at depth. Most of the warm-to-cold transformation takes place east of Greenland (Lozier et al., 2019; Petit et al., 2020). The bulk of the deep return flow is composed of dense overflow plumes from the Nordic Seas, together with the water masses they entrain while descending from gaps in the Greenland–Scotland Ridge to the abyss of the North Atlantic (Chafik and Rossby, 2019). The exchange flow of warm and cold water masses across the ridge is reasonably well known (Østerhus et al., 2019; Tsubouchi et al., 2021), but open questions remain regarding where and how the water mass transformation north of the ridge takes place.

Swift et al. (1980) and Swift and Aagaard (1981) proposed that the overflow water through Denmark Strait, which forms the densest contribution to the lower limb of the overturning circulation, originates via open-ocean convection in the Iceland Sea. They used hydrographic properties and chemical tracers to match dense water in the Denmark Strait overflow plume with wintertime mixed layers in the Iceland Sea, and applied a volumetric approach to determine the hydrographic properties of the locally formed water mass. Formation of a similar water mass in the central Greenland Sea was documented some years later (Strass et al., 1993). By contrast, subsequent work emphasized water mass transformation within the boundary current system around the Nordic Seas and the supply to Denmark Strait via the East Greenland Current (Fig. 1; Mauritzen, 1996). Consequently, open-ocean convection in the Iceland and Greenland Seas was eventually discounted as an important source of Denmark Strait overflow water. Among the main reasons for that were the interannual and seasonal variability of the production that are not manifest in the overflow transport as well as the lack of a known direct pathway from the interior basins. Intermediate water formed in the Iceland and Greenland Seas was instead thought to supply the other major overflow from the Nordic Seas through the Faroe Bank Channel (Mauritzen, 1996).

* Corresponding author.
*E-mail address:* kjetil.vage@uib.no (K. Våge).

https://doi.org/10.1016/j.dsr.2022.103824
Received 11 August 2021; Received in revised form 1 June 2022; Accepted 3 June 2022
Available online 13 June 2022

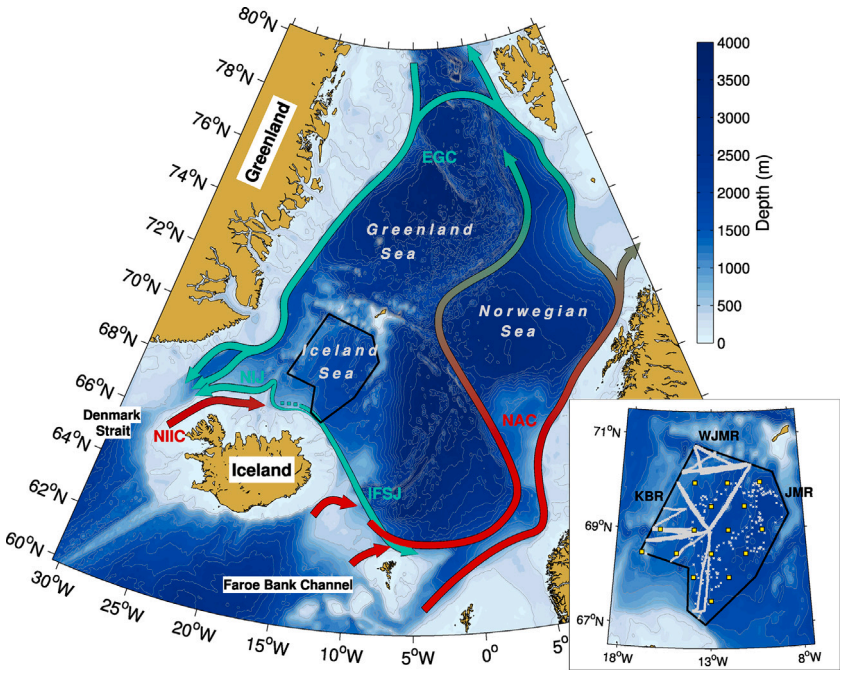


**Fig. 1.** Schematic of the major currents in the Nordic Seas. The change in color indicates the gradual warm-to-cold transformation of the Atlantic inflow as it progresses northward from the Greenland–Scotland Ridge. The central Iceland Sea control volume used in the volumetric analysis is outlined in black. The dashed portion of the IFSJ indicates its uncertain origin. The inset shows the data used in the volumetric analyses and the submarine ridges enclosing the control volume. The yellow squares and gray dots are measurements from winters 1974–75 and 2015–16, respectively. The acronyms are: EGC = East Greenland Current; NIJ = North Icelandic Jet; IFSJ = Iceland–Faroe Slope Jet; NIIC = North Icelandic Irminger Current; NAC = Norwegian Atlantic Current; KBR = Kolbeinsey Ridge; WJMR = West Jan Mayen Ridge; JMR = Jan Mayen Ridge.

We now know that approximately equal amounts of dense water pass across the Greenland–Scotland Ridge east and west of Iceland (Østerhus et al., 2019). Much of this overflow water is transported by currents originating in the Iceland Sea. The North Icelandic Jet (NIJ, Fig. 1) flows westward along the 600–800 m isobaths on the slope north of Iceland into Denmark Strait (Jónsson and Valdimarsson, 2004; Våge et al., 2011; Pickart et al., 2017; Semper et al., 2019). The NIJ supplies approximately one third to one half of the overflow through Denmark Strait, including the densest component (Harden et al., 2016; Semper et al., 2019). The Iceland–Faroe Slope Jet (IFSJ, Fig. 1) flows eastward along the Iceland–Scotland Ridge toward the Faroe Bank Channel at slightly greater depth than the NIJ, which is consistent with a deeper sill compared to Denmark Strait (Semper et al., 2020; Chafik et al., 2020). The hydrographic properties of the dense waters transported by the NIJ and IFSJ are similar, suggesting that the currents share a common source (Semper et al., 2020). In the present climate these dense waters primarily originate in the Greenland Sea (Huang et al., 2020), while the water formed in the Iceland Sea for the most part is not sufficiently dense (Våge et al., 2015).

A substantial portion of the water mass transformation in the Iceland and Greenland Seas is driven by strong air-sea heat fluxes during cold-air outbreaks (Papritz and Spengler, 2017; Våge et al., 2015). The most intense cooling occurs along the marginal ice zone, where cold, dry air first encounters open water. As the climate has warmed, the sea-ice extent in the Nordic Seas has decreased and the ice edge has receded from the interior basins toward the coast of Greenland. This has resulted in diminished heat fluxes in the Iceland and Greenland Seas and reduced convection in the interior basins (Moore et al., 2015), but at the same time has permitted ventilation within the East Greenland Current (Våge et al., 2018; Renfrew et al., 2019; Huang et al., 2021; Moore et al., 2022). Here we demonstrate that the role of dense-water formation in the Iceland Sea as part of the overturning in the Nordic Seas has significantly changed, by contrasting the winters of 1974–75 and 2015–16 that are separated by more than four decades.

## 2. Data and methods

### 2.1. Hydrographic data

We utilize the volumetric approach of Swift and Aagaard (1981) to quantify water mass transformation in the Iceland Sea. They applied the technique to hydrographic data obtained during surveys of the ice-free portions of the Iceland Sea in October–November 1974 and February–March 1975 (Fig. 1). Winter 2015–16 is the only winter since then with sufficient spatial data coverage to repeat this volumetric analysis. The hydrographic data from winter 2015–16 were primarily obtained by three autonomous ocean gliders that operated in the Iceland Sea from August 2015 to May 2016 (Fig. 1). The gliders sampled the upper 1000 m of the water column with a vertical resolution of 1–5 m, enhanced within the surface mixed layer. Details of the processing and calibration of the glider data are provided in Våge et al. (2018). Additional hydrographic data from the monitoring cruises of the Marine and Freshwater Research Institute of Iceland and from the Argo global program of profiling floats from the same time period were included to augment the glider data set. Only delayed-mode data from the Argo program, which have been corrected for drift in the pressure and conductivity sensors (Wong et al., 2003), were used.

To calibrate the Argo data, we identified a subset of Argo profiles that were obtained within 10 days and 50 km from shipborne conductivity-temperature-depth (CTD) profiles. These Argo-CTD profile pairs revealed a fresh bias of approximately 0.002 g/kg in the Argo profiles. Substantial near-surface variability masked the bias in the upper 400 m; below that depth the bias was depth-independent. This bias is well below the accuracy of 0.01 PSS-78 in salinity for the Argo program (Wong et al., 2020) and not rectified by the delayed-mode quality control, but would impact the volumetric analysis. To correct for the bias, a constant, depth-independent offset corresponding to the mean difference below 500 m between each Argo profile and a mean central Iceland Sea profile computed from the shipborne CTD data was calculated. This offset was applied to 112 of 178 Argo profiles from

4 of 6 active floats in the Iceland Sea that differed by more than three standard deviations from the mean central Iceland Sea profile.

Prior to the volumetric calculations, each profile was interpolated onto a standard 800 m vertical grid with 1 m resolution. A 5-m median filter was applied to remove spikes from the profiles.

A historical hydrographic data set spanning the period 1950–present (Huang et al., 2020) was used to assess the long-term variability in the central Iceland Sea, in particular the change from winter 1974–75 to winter 2015–16. The data set contains profiles from ships, Argo floats, and gliders. Prior to the first Argo float deployment in 2005 the mean number of profiles each year was about 40. After 2005 this number nearly quadrupled. The vertical resolution in the upper 800 m gradually increased from around 60 m before the early 1970s to less than 10 m after the mid-1990s.

### 2.2. Volumetric analysis

A volumetric analysis quantifies temporal changes in the proportions of different water masses within a control volume (e.g., Swift and Aagaard, 1981; Yashayaev, 2007; Brakstad et al., 2019). The black polygon in Fig. 1 outlines the central Iceland Sea control volume used in our volumetric analysis. A set of submarine ridges (Kolbeinsey Ridge to the west, West Jan Mayen Ridge to the north, and Jan Mayen Ridge to the east) as well as the north Iceland slope to the south provide natural boundaries. The southeasternmost part of the Iceland Sea was not included in the domain due to a lack of data from this region in winter 2015–16. The mixed layers in the southeastern region are shallower and less dense than in the rest of the Iceland Sea (Våge et al., 2015), hence the omission only reduced our volumetric estimates of water mass transformation in the lightest density classes.

For winter 2015–16 a regular 0.5° longitude by 0.2° latitude grid was constructed within these boundaries. An effective radius of 75 km (corresponding to nearly 2 degrees of longitude in this latitude band) was assigned to each grid point. Following the procedure of Davis (1998) and Våge et al. (2013), the effective radius was increased along isobaths in regions of large topographic gradients to take into account the greater length scales along the bottom topography. This is appropriate given the close alignment between the circulation in the Nordic Seas and the bottom topography (e.g., Nøst and Isachsen, 2003). Bathymetric data were obtained from the ETOPO 1-min elevation data base (Amante and Eakins, 2009) and smoothed by convolution with a 10 km Gaussian window. Within the effective radius around each grid point, all profiles obtained within a 10-day window were averaged to reduce the influence of periods of heavy sampling. Finally, distance-weighted mean profiles and their standard deviations (for grid points with at least 5 profiles) for the months of September–November and February–April were calculated at each node. To avoid near-surface data gaps we assumed a mixed-layer depth of at least 10 m and extrapolated each mean profile from a depth of 10 m to the surface. Data gaps at depth were filled using linear interpolation from nearby grid points (only one late-winter grid point required such interpolation, at depths below 700 m). The resulting 3-dimensional gridded fields of Absolute Salinity, Conservative Temperature, and potential density anomaly (hereafter referred to as salinity, temperature, and density) for September–October and February–April are designated fall and late winter, respectively. The fall data were obtained prior to the onset of wintertime convection, and the late-winter data were recorded when the mixed layers are deepest and densest (Våge et al., 2015). At most grid points multiple profiles were collected over the 3-month periods in fall and late winter. We computed standard deviations at each grid point to account for the temporal variability, then combined these standard deviations to address the spatial variability across the control volume. From this we estimated upper and lower bounds of the volumetric inventory in each density class, which formed the basis for the error estimates.

For winter 1974–75, the fall and late-winter data from the central Iceland Sea (Fig. 1) were obtained between late October and early November 1974 and between late February and early March 1975, respectively. Both data sets were collected within 10-day periods. Due to the relatively low spatial resolution of the winter 1974–75 hydrographic surveys, a regular 1° longitude by 0.5° latitude grid was constructed within the same boundaries as for winter 2015–16. The results are not sensitive to the resolution of the grid. The surveys alone did not provide sufficient data to compute standard deviations at each grid point for error estimates. Taking advantage of the synopticity of the fall 1974 and late winter 1975 surveys, we instead considered the standard deviation of all profiles within the central Iceland Sea control volume as an estimate of the lateral variability. The coarser vertical resolution was taken into account by vertically shifting the mean central Iceland Sea profiles by half of the mean vertical resolution above the $\sigma_\theta$ = 28.05 kg/m$^3$ isopycnal of 28 m in both directions, then using the differences between the resulting profiles to form envelopes of uncertainty (the mean vertical resolution of the profiles from winter 2015–16 was less than 3 m). These differences were substantial in the pycnocline, where the hydrographic properties had a pronounced gradient, but considerably reduced where the profiles were more uniform. The two error source terms were combined as the root of the sum of the squares. Otherwise, interpolated fields of temperature, salinity, and potential density were computed the same way as for winter 2015–16.

### 2.3. Reanalysis data

We used the ERA5 reanalysis, which is the fifth generation atmospheric reanalysis product from the European Centre for Medium-Range Weather Forecasts. It extends back to 1950 and has a spatial resolution of approximately 31 km (Hersbach et al., 2020; Bell et al., 2021). We used sea-ice concentration and surface turbulent fluxes from the ERA5 data set. The turbulent fluxes are generally in good agreement with observations over the ice-free ocean, but less accurate over the marginal ice zone. This is primarily due to an overly smooth sea-ice distribution in the ERA5 surface boundary conditions (Renfrew et al., 2021).

## 3. Water mass transformation in winter 2015–16

The collection of hydrographic profiles from the central Iceland Sea in winter 2015–16 is shown in Fig. 2a. The mean temperature, salinity, and density profiles illustrate the seasonal transition from relatively warm, shallow mixed layers in fall to colder, denser, and deeper mixed layers in late winter. Typical wintertime mixed-layer depths were in the range 150–250 m (Fig. 2a; see also Våge et al., 2015). All of the late-winter mixed layers had densities greater than $\sigma_\theta$ = 27.8 kg/m$^3$, typically taken to delimit overflow water (Dickson and Brown, 1994). As such, dense water masses formed in the Iceland Sea may be regarded as potential contributors to the overflow plumes across the Greenland–Scotland Ridge (Våge et al., 2015).

To further quantify the seasonal water mass transformation in the Iceland Sea, we conducted a volumetric analysis as outlined in the Data and methods section (e.g., Swift and Aagaard, 1981). The temperature and salinity fields were partitioned into 0.1 °C by 0.005 g/kg classes for fall and late winter (Fig. 3). Following Swift and Aagaard (1981) we only integrated down to the $\sigma_\theta$ = 28.05 kg/m$^3$ isopycnal (approximately 600 m depth), which is not ventilated in the Iceland Sea in winter. As indicated by the spread of the fall profiles (Fig. 2a), warm and fresh surface water masses were prevalent, mostly from the early part of the fall period and the southern part of the central Iceland Sea. At depth the profiles were more uniform, which is reflected by increasing volumes of a narrow subset of temperature–salinity classes at higher densities (Fig. 3a). At the end of winter 2015–16 there was hardly any water less dense than $\sigma_\theta$ = 27.9 kg/m$^3$ in the central Iceland Sea (Fig. 3b). While some of the fresh surface water in the western Iceland Sea is advected toward Greenland in fall and winter

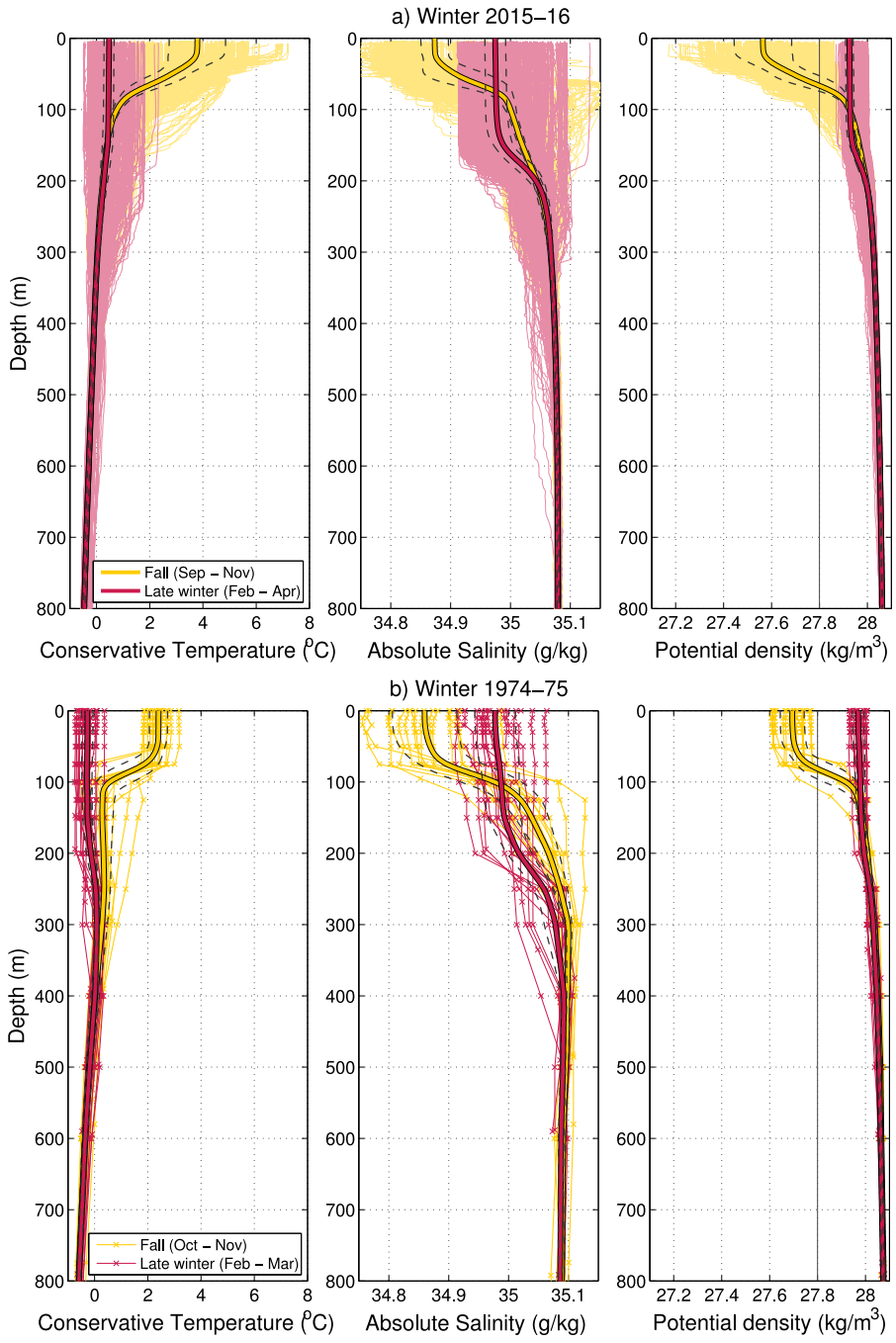


**Fig. 2.** Central Iceland Sea hydrographic profiles from winter 2015–16 (a) and winter 1974–75 (b). The yellow profiles represent fall and the red profiles winter. The thick and dashed lines are the means and standard deviations (taking also into account the reduced vertical resolution for winter 1974–75 as detailed in the Data and methods section), respectively. The vertical gray lines represent the $\sigma_\theta$ = 27.8 kg/m$^3$ isopycnal.

by westward Ekman transport induced by strong northerly winds (Våge et al., 2018; Spall et al., 2021), most of the light surface water is transformed into denser water (Swift and Aagaard, 1981; Våge et al., 2015). The difference between the late-winter and fall inventories shows an increase in volume denser than $\sigma_\theta$ = 27.9 kg/m$^3$, in particular at salinities near 34.95 g/kg (Fig. 3c). This was the main water mass formed in the central Iceland Sea in winter 2015–16, which would be classified as upper Arctic Intermediate Water according to Swift and Aagaard (1981).

The 2015–16 fall and late-winter volumetric inventories were also divided into 0.01 kg/m$^3$ density classes (Fig. 4a). Water less dense than the overflow water limit of $\sigma_\theta$ = 27.8 kg/m$^3$ constituted a substantial portion (11%) of the fall inventory, only the two highest-density classes were more voluminous ($\sigma_\theta$ = 28.04–28.05 kg/m$^3$, yellow bars in Fig. 4a). Consistent with Fig. 3b, there were only negligible amounts of water less dense than $\sigma_\theta$ = 27.9 kg/m$^3$ in the central Iceland Sea in late winter (red bars). The fall and late-winter inventories were nearly identical for the densest classes, which are not affected by the seasonal water mass transformation (Våge et al., 2015). In the density range $\sigma_\theta$ = 27.90–27.95 kg/m$^3$ (highlighted in Fig. 4a by the dashed lines) the inventory increased from fall to winter by 9000 ± 4000 km$^3$, primarily due to local water mass transformation. Considering the time interval between the fall and late-winter periods of approximately five months, the difference in inventory can be converted to a net formation rate of 0.7 ± 0.3 Sv (1 Sv ≡ 10$^6$ m$^3$/s). This estimate does not take into account flow into and out of the central Iceland Sea. Assuming that water in this

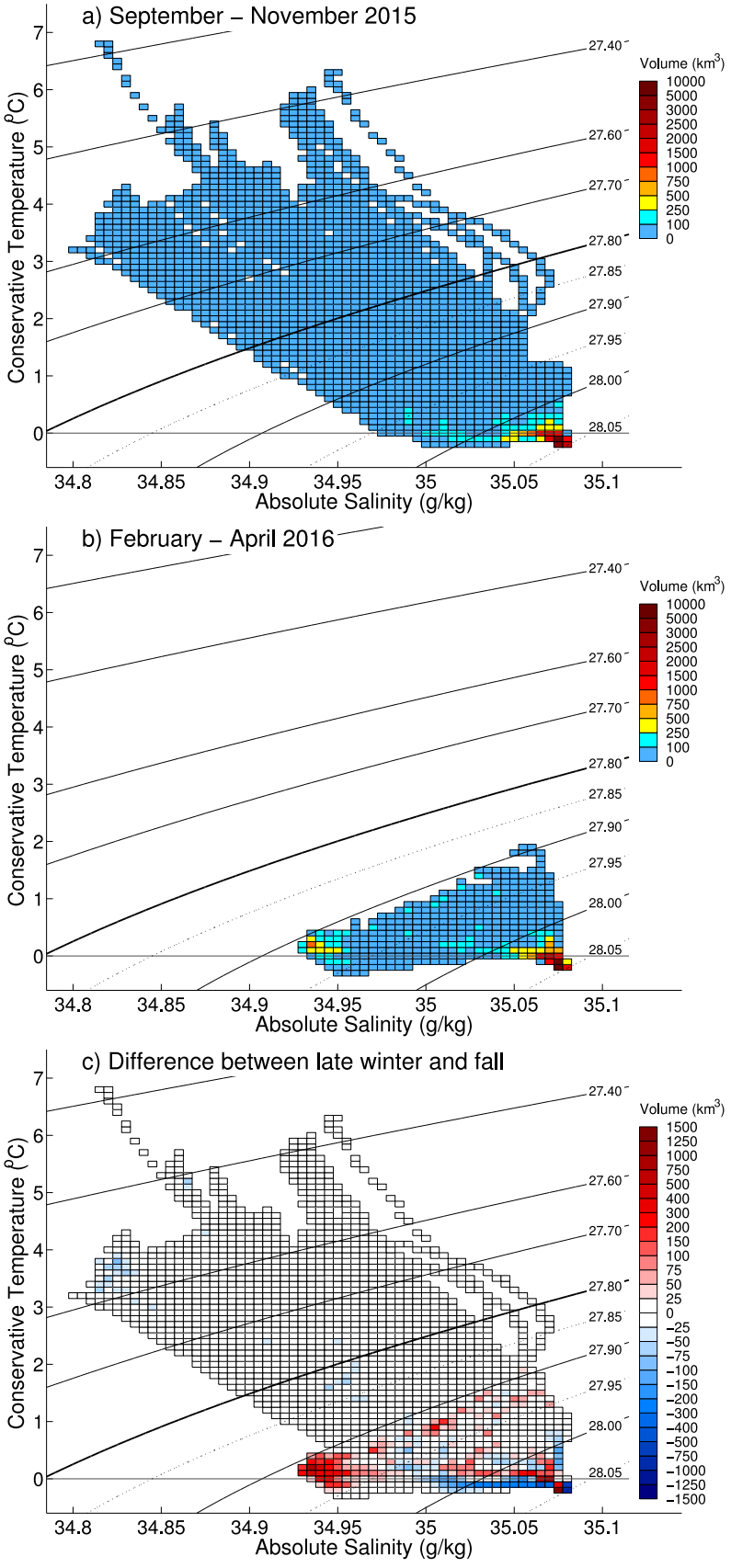


**Fig. 3.** Volumetric inventories in temperature–salinity space for winter 2015–16. The panels show the volume of water less dense than $\sigma_\theta$ = 28.05 kg/m$^3$ within the black outline in Fig. 1 for fall (a, Sep–Nov), late winter (b, Feb–Apr), and the difference in volume between late winter and fall (c). The horizontal gray line in each panel represents the 0 °C isotherm.

density range is exported from the Iceland Sea throughout the year, this formation rate is likely an underestimate. In terms of volume transport, 0.7 ± 0.3 Sv would constitute a substantial proportion of the more than 1.8 ± 0.3 Sv of potential overflow water transported by the NIJ upstream of Denmark Strait (Semper et al., 2019). However, most of that transport is composed of water substantially denser than the dense water formed in the central Iceland Sea in winter 2015–16 (blue bars in Fig. 4). The total NIJ transport in the density range $\sigma_\theta$ = 27.90–27.95 kg/m$^3$ is less than 0.2 Sv. As such, water mass transformation in the Iceland Sea is not an important source of dense water for the NIJ and the IFSJ in the present climate.

We note that in the density range $\sigma_\theta$ = 27.98–28.02 kg/m$^3$ the inventory was greater in fall than in late winter. This range represents density classes that are continuously drained from the Iceland Sea by the NIJ and IFSJ, but not replenished at the same rate. However, water in these density classes is regularly formed just outside the borders of the central Iceland Sea (e.g., Våge et al., 2018; Huang et al., 2021). Using a collection of historical hydrographic measurements dating back to 1980 (Huang et al., 2020), we computed the thickness of the $\sigma_\theta$ = 27.90–27.95, 27.98–28.02, and 28.03–28.05 kg/m$^3$ density ranges (i.e., the mean difference in depth between the upper and lower bounds of the density intervals, not shown). For the first range, which represents the main product of local water mass transformation, a pronounced seasonal signal with maximum thickness in April was evident. The second range, where the volumetric inventory was reduced from fall to winter, also had a seasonal signal, but the maximum thickness was delayed from April to May. This likely implies a delayed influx of newly formed dense water through the northern boundary of the central Iceland Sea, which subsequently drains through the southern boundary at a constant rate. The final range, representing the densest classes whose inventory remained unchanged from fall to late winter and was not ventilated in the Iceland Sea in winter 2015–16, did not have a seasonal signal in layer thickness. As the NIJ and IFSJ transport substantial amounts of water in these density classes, the flow into and out of the central Iceland Sea in this density range must be nearly constant.

## 4. Water mass transformation in winter 1974–75

Swift and Aagaard (1981) conducted a similar volumetric analysis for the ice-free portion of the Iceland Sea in winter 1974–75. To quantitatively compare the winters of 1974–75 and 2015–16, we repeated their volumetric analysis for the central Iceland Sea control volume (Fig. 1). The winter 1974–75 profiles are qualitatively similar to the winter 2015–16 profiles (Fig. 2). In particular, mixed-layer depths of 150–300 m match well, though the lower vertical resolution prevents accurate comparison. However, the winter 1974–75 mixed layers were notably colder and denser.

The volumetric inventory (Fig. 4b) shows that also in winter 1974–75 nearly all surface water less dense than $\sigma_\theta$ = 27.9 kg/m$^3$ was either flushed out of the central Iceland Sea or transformed into denser classes. In contrast to winter 2015–16, most of the gain in inventory from the 1974 fall survey to the 1975 late-winter survey took place within the significantly higher $\sigma_\theta$ = 27.96–28.01 kg/m$^3$ density range (highlighted in Fig. 4b by the dashed lines). Taking into account the time difference between the fall and the late-winter surveys of approximately 4 months, we estimate a net formation rate of 0.8 ± 0.3 Sv — nearly the same as for winter 2015–16. Unlike winter 2015–16, the hydrographic data from winter 1974–75 were obtained from synoptic surveys, which is the main reason the uncertainties are similar despite the lower spatial and vertical resolutions in winter 1974–75.

The NIJ transport by density class (blue bars in Fig. 4) was calculated from data obtained between 2004 and 2018. While the NIJ has become warmer and more saline since the mid-1990s (Pickart et al., 2017), the changes in temperature and salinity have largely been density compensated. Since monitoring of the Denmark Strait overflow commenced in 1996, the overflow water transport has been remarkably steady (Jochumsen et al., 2017). Hydrographic measurements from Denmark Strait dating back to the 1950s show that the density of the overflow water has hardly changed (Smedsrud et al., 2022). If the dynamics governing the NIJ involving an up-tilt of dense isopycnals along the slope north of Iceland (Våge et al., 2011; Semper et al., 2019) were not substantially different, it is possible that the density structure of the 1970s NIJ may resemble that of the present. If that holds, Fig. 4b indicates that water mass transformation in the central Iceland Sea may have been a more important source to the NIJ, and hence of dense water to Denmark Strait, in past climates than it is today.

The late-winter survey in 1975 took place from late February to early March. This is 1–2 months before the mixed layers typically reach their maximum depth and density (Våge et al., 2015). Estimates using a one-dimensional mixed-layer model (Price et al., 1986) integrated for 1.5 months subject to a constant heat loss of 150 W/m$^2$ (corresponding to the mean ocean-to-atmosphere turbulent and radiative fluxes from late February to mid-April), indicate that the mean end-of-winter mixed-layer density would increase by approximately 0.03 kg/m$^3$ to 28.00 kg/m$^3$. Swift and Aagaard (1981) surmised that water as dense as 28.05 kg/m$^3$ may have formed in the Iceland Sea by the end of that winter. Assuming that such an increase applied to all density classes in the Iceland Sea volumetric inventory (Fig. 4b) and that the density structure of the NIJ was not substantially altered from the 1970s to the present, we conclude that the Iceland Sea was likely an important source to the NIJ and the Denmark Strait overflow in winter 1974–75.

## 5. Long-term variability in the central Iceland Sea

By contrasting winters 1974–75 and 2015–16, we have demonstrated that mixed-layer depths and net dense-water formation rates have not changed appreciably, while the mixed layers have become warmer and less dense over the intervening four decades. In particular, a substantial portion of the water formed in the central Iceland Sea is now warmer than 0 °C (Figs. 2a and 3c). Swift and Aagaard (1981) referred to the central Iceland and Greenland Seas — the region limited by the Arctic Front to the east and the Polar Front to the west — as the Arctic domain. The intermediate water masses formed in this region are considered Arctic-origin waters (e.g., Våge et al., 2011; Mastropole et al., 2017) and characterized by a temperature below 0 °C. While such water is still formed in the Greenland Sea (e.g., Brakstad et al., 2019), most of the water ventilated in the Iceland Sea in winter 2015–16 was warmer than 0 °C. This is not unexpected in the present climate. Hence using the 0 °C isotherm to distinguish intermediate waters of Arctic origin and Atlantic origin (formed east of the Arctic Front; Swift and Aagaard, 1981) should be done with caution.

Furthermore, below the mixed layer the water column has become less dense. Since 1950, isopycnals in the intermediate part of the water column in the central Iceland Sea have descended, the deeper isopycnals to a greater extent than the shallower isopycnals (Fig. 5). This implies that the intermediate layer has become less stratified. For water mass transformation in the Iceland Sea this has little impact, since convection is typically limited to depths of about 200 m with mixed-layer densities lower than these descending isopycnals (Våge et al., 2015). More importantly, the descending isopycnals also mean that the densest components of the water supplying the overflows across the Greenland–Scotland Ridge are located at substantially deeper levels now than in previous decades. Consider in particular the $\sigma_\theta$ = 28.05 kg/m$^3$ isopycnal, which corresponds to the "transport mode" of the NIJ (i.e., the most voluminous class of water transported by the current, Semper et al., 2019). In the 1950s this isopycnal was on average located just below 300 m depth, while the mean depth of the same isopycnal was nearly 600 m in the 2010s. This echoes the findings of Våge et al. (2015) from a repeat hydrographic station off northeast Iceland, except that the descent appears more gradual in the present longer-term perspective. These descending isopycnals have implications for the

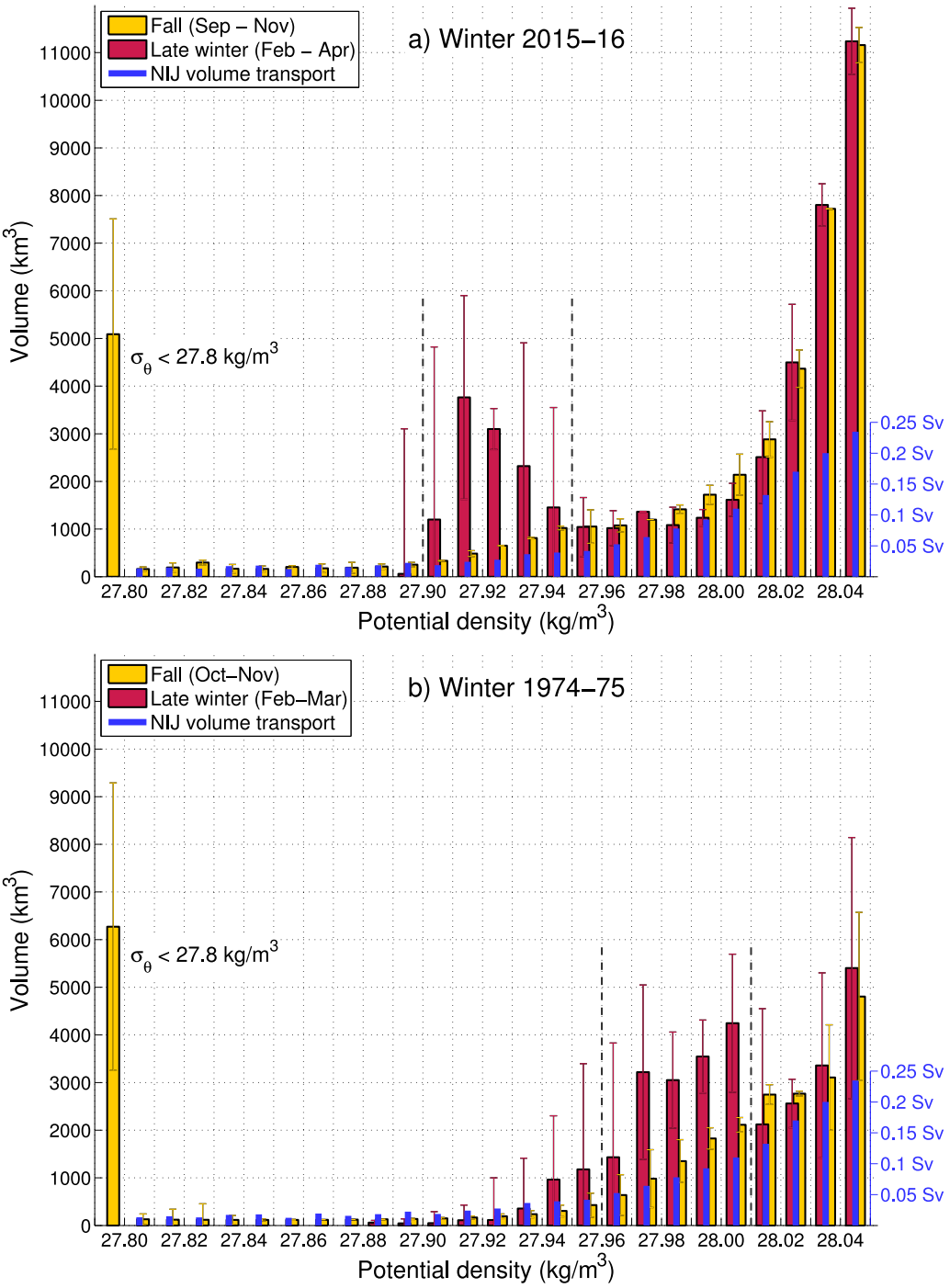


**Fig. 4.** Volumetric inventories divided into density classes of width 0.01 kg/m$^3$ for winter 2015–16 (a) and winter 1974–75 (b). The yellow bars represent inventories from fall and the red bars from late winter. The blue bars, scaled by the blue axis on the right side of the figure, are North Icelandic Jet volume transports (representative of the period 2004–18) divided into the same density classes (Semper et al., 2019). The vertical dashed lines enclose the density interval in which most of the local water mass transformation took place each winter.

supply of the densest components of the overflow water, transported from the Iceland Sea to Denmark Strait by the NIJ and to the Faroe Bank Channel by the IFSJ.

The root cause of the descending isopycnals in the central Iceland Sea (Fig. 5) is reduced formation of dense intermediate water, which is being replaced by less dense intermediate water. Relative to the 1950s, the upper 800 m of the water column have become warmer and less saline (not shown). Lower salinities and higher temperatures were the main causes of reduced density between 1980 and 2000 and in the 2010s, respectively. The recent warming in the Iceland Sea mirrors that in the Greenland Sea (Lauvset et al., 2018; Brakstad et al., 2019).

## 6. Diminishing air-sea heat loss

Using the ERA5 reanalysis product, we computed the ocean to atmosphere turbulent heat fluxes in the central Iceland Sea (Fig. 6). While the fluxes were generally higher prior to the early 1980s compared to the latter part of the record, there was pronounced interannual

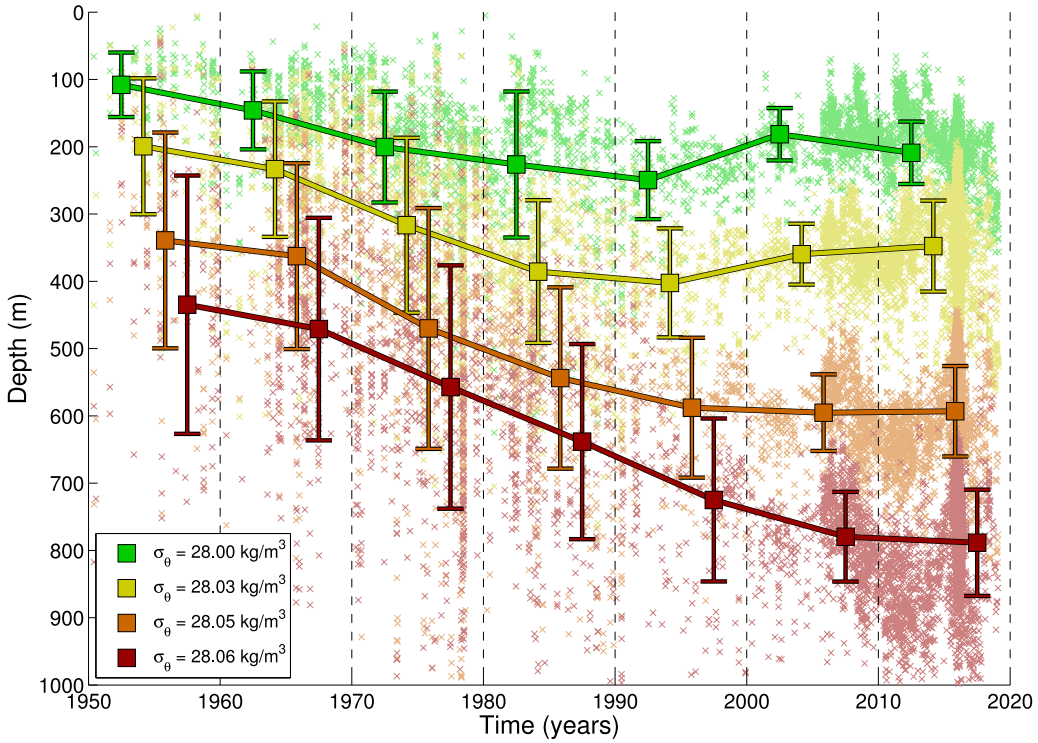


**Fig. 5.** Evolving density structure in the central Iceland Sea (Fig. 1) from 1950 to present. Depths of the $\sigma_\theta$ = 28.00, 28.03, 28.05, and 28.06 kg/m$^3$ isopycnals for each hydrographic profile in the central Iceland Sea are marked by green, yellow, orange, and red crosses, respectively. Decadal means and standard deviations are indicated by the squares and error bars. Note that while each mean and standard deviation represent the decade indicated by the vertical dashed lines, they are staggered to avoid overlapping symbols.

variability. Winter 1974–75 was among the most severe winters of the past 70 years. Winter 2015–16 was substantially weaker, but representative of the past 20–30 winters. Moore et al. (2015) attributed the overall diminishing heat loss to a reduction in the air-sea temperature difference and retreat of the sea-ice edge toward Greenland.

Cold-air outbreaks, atmospheric events where cold, dry polar air is advected over the comparatively warm ocean, are responsible for most of the wintertime heat loss in the Nordic Seas (Våge et al., 2015; Papritz and Spengler, 2017; Terpstra et al., 2021). The strongest heat loss takes place near the sea-ice edge, where the cold air first encounters open water (e.g., Spensberger and Spengler, 2021). In accordance with the retreating ice edge, the region of highest heat loss has migrated from the central Iceland Sea toward Greenland (Moore et al., 2015; Pope et al., 2020). In the 1970s the western Iceland Sea was covered by sea ice in winter and the ice edge was located near Kolbeinsey Ridge, bordering the central Iceland Sea (Fig. 7b). The frigid polar air emanating from the ice-covered region during cold-air outbreaks efficiently extracted heat from the central Iceland Sea. By contrast, in the 2010s the ice edge had retreated toward the Greenland shelf break, and much of the western Iceland Sea was ice-free in winter. Consequently, during cold-air outbreaks the polar air had already been modified by air-sea interaction prior to arriving over the central Iceland Sea, contributing to the recent reduction in heat loss.

In February 2016, convection to depths of 400–500 m with mixed-layer densities of 28.01–28.02 kg/m$^3$ took place to the west of Kolbeinsey Ridge, in an area that until recently had been within the marginal ice zone in winter (Våge et al., 2018). This is outside of the control volume considered above, and the hydrographic conditions here are different than in the central Iceland Sea. The convection in the western Iceland Sea in winter 2015–16 re-ventilated the Atlantic-origin water transported by the East Greenland Current, resulting in a denser product than the Arctic-origin water formed in the central Iceland Sea in winter 1974–75 (Fig. 4b). From Fram Strait to Denmark Strait the ice-edge retreat has exposed long stretches of the East Greenland Current to enhanced heat loss in winter (Moore et al., 2022). This indicates that, if properly pre-conditioned by strong northerly winds in fall and winter that shift the buoyant surface water toward Greenland (Våge et al., 2018; Spall et al., 2021), very dense water may form near the ice edge in the western Iceland and Greenland Seas. The recent numerical simulations of Wu et al. (2021) support this notion.

## 7. Discussion and conclusions

The volumetric analysis applied here is a powerful method to determine changes in water mass volumes between two periods, in particular to identify the product of water mass transformation when applied before and after winter convection. Such a volumetric analysis presumes that there is no advection into and out of the control volume. This is not the case for the central Iceland Sea, from which dense water is continuously exported by the NIJ and IFSJ. As such, the estimates of net formation rates, which take into account the time that passed between the fall and late-winter measurements, are likely biased low and should therefore be considered conservative estimates. This applies in particular to winter 1974–75, when denser water that more closely matched the properties of the NIJ was formed. While the volumetric inventories were only assessed for winters 1974–75 and 2015–16, when the spatial data coverage was sufficient, comparison of mixed-layer properties and hydrographic structure with other winters within the same decades indicates that the two winters are broadly representative.

Unless the density structure of the NIJ substantially changed, our volumetric analysis revealed that the central Iceland Sea was a more important source of dense water to the NIJ in the 1970s than it is today. Although the net formation rates and convection depths were comparable for winters 1974–75 and 2015–16, the mixed-layer densities declined over the intervening four decades to the extent that the NIJ transports negligible amounts of water in the density range that is presently the main product of water mass transformation in the Iceland Sea ($\sigma_\theta$ = 27.90–27.95 kg/m$^3$). This begs the question: what happens to

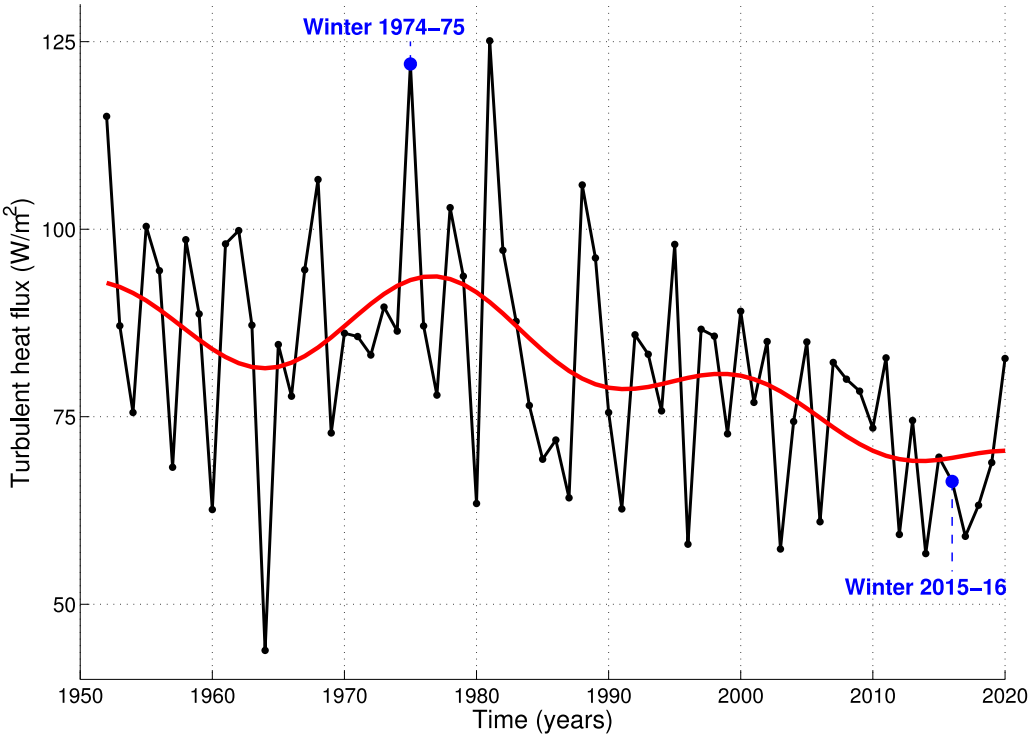


**Fig. 6.** Total turbulent (sensible plus latent) heat flux from the central Iceland Sea (Fig. 1). The black line shows the mean fluxes averaged over the winter period of October through April. Winters 1974–75 and 2015–16 are marked in blue. The red line is the sum of the first two components of the Fourier transform representing variability with periods greater than 35 years.

the dense water presently formed in the Iceland Sea? This water mass is sufficiently dense to contribute to the overflows from the Nordic Seas. Hydro-chemical analyses indicate that it is an important component both of the overflows east of Iceland (Fogelqvist et al., 2003) and of the intermediate water in the Norwegian Sea (Jeansson et al., 2017). (We note that the East Icelandic Current offers a direct pathway from the Iceland Sea to the Norwegian Sea, Macrander et al., 2014; de Jong et al., 2018).

Most of the densest waters flowing into Denmark Strait and the Faroe Bank Channel likely pass through the Iceland Sea (Våge et al., 2011; Semper et al., 2019, 2020; Huang et al., 2020). Since 1950 these dense water masses have been located at increasing depth in the central Iceland Sea and hence are becoming less readily available to supply the NIJ and IFSJ. Descending isopycnals are not unique to the Iceland Sea; this has been reported across all basins of the Nordic Seas (e.g., Turrell et al., 1999; Mork et al., 2014; Brakstad et al., 2019). This implies that the reservoir of water that supplies the densest portion of the overflows from the Nordic Seas is diminishing, while dynamical constraints already limit its effective capacity (Yang and Pratt, 2013). Since monitoring commenced in the 1990s, the transport of overflow waters from the Nordic Seas has been remarkably steady (Østerhus et al., 2019). This stability may not continue if these dense water masses are renewed at a rate slower than they are removed by the overflows. The NIJ and IFSJ transport dense water from the interior brought to the Iceland slope by shelf-basin interaction (Våge et al., 2011; Semper et al., 2019, 2020; Huang et al., 2020). This mechanism may become less efficient as dense-water formation declines.

Over the four decades separating the two winters of 1974–75 and 2015–16, the role of the Iceland Sea in the overturning in the Nordic Seas has undergone a remarkable change. In the mid-1970s sufficiently dense water to supply the NIJ — ultimately the densest contribution from the Nordic Seas to the lower limb of the Atlantic Meridional Overturning Circulation — was formed in the Iceland Sea. Four decades later, in the present climate, the central Iceland Sea is no longer an important source of dense water to the NIJ. However, due to ice-edge retreat toward Greenland, re-ventilation of Atlantic-origin water in the East Greenland Current now occurs during its transit through the western Iceland Sea in winter (Våge et al., 2018; Renfrew et al., 2019; Huang et al., 2021). This additional densification of water contributing to the overflow through Denmark Strait may to some extent compensate the reduced reservoir of dense water in the interior basins of the Nordic Seas. To predict how the overturning in the Nordic Seas will continue to respond to a warming climate, it is imperative to better understand and quantify how the effective capacity of the dense-water reservoir in the Nordic Seas is developing, as well as the extent that the Atlantic-origin water in the East Greenland Current is densified during transit through the ice-free portions of the western Greenland and Iceland Seas in winter.

## Data availability

The glider data can be accessed at the Pangaea repository (doi:10.1594/PANGAEA.884339). The profiling float data were collected and made freely available by the international Argo project and the national programs that contribute to it (doi:10.17882/42182). The combined hydrographic data set is available on request. The ERA5 reanalysis data were obtained from the European Centre for Medium-Range Weather Forecasts.

## Acknowledgments

Support for this work was provided by the Trond Mohn Foundation, Norway under grant BFS2016REK01 (K.V. and S.S.), the European Union's Horizon 2020 research and innovation programme under the Marie Skłodowska-Curie grant agreement no. 101022251 (S.S.), the US National Science Foundation under grants OCE-1259618 and OCE-1948505 (R.S.P), and the Natural Sciences and Engineering Research Council of Canada (G.W.K.M).

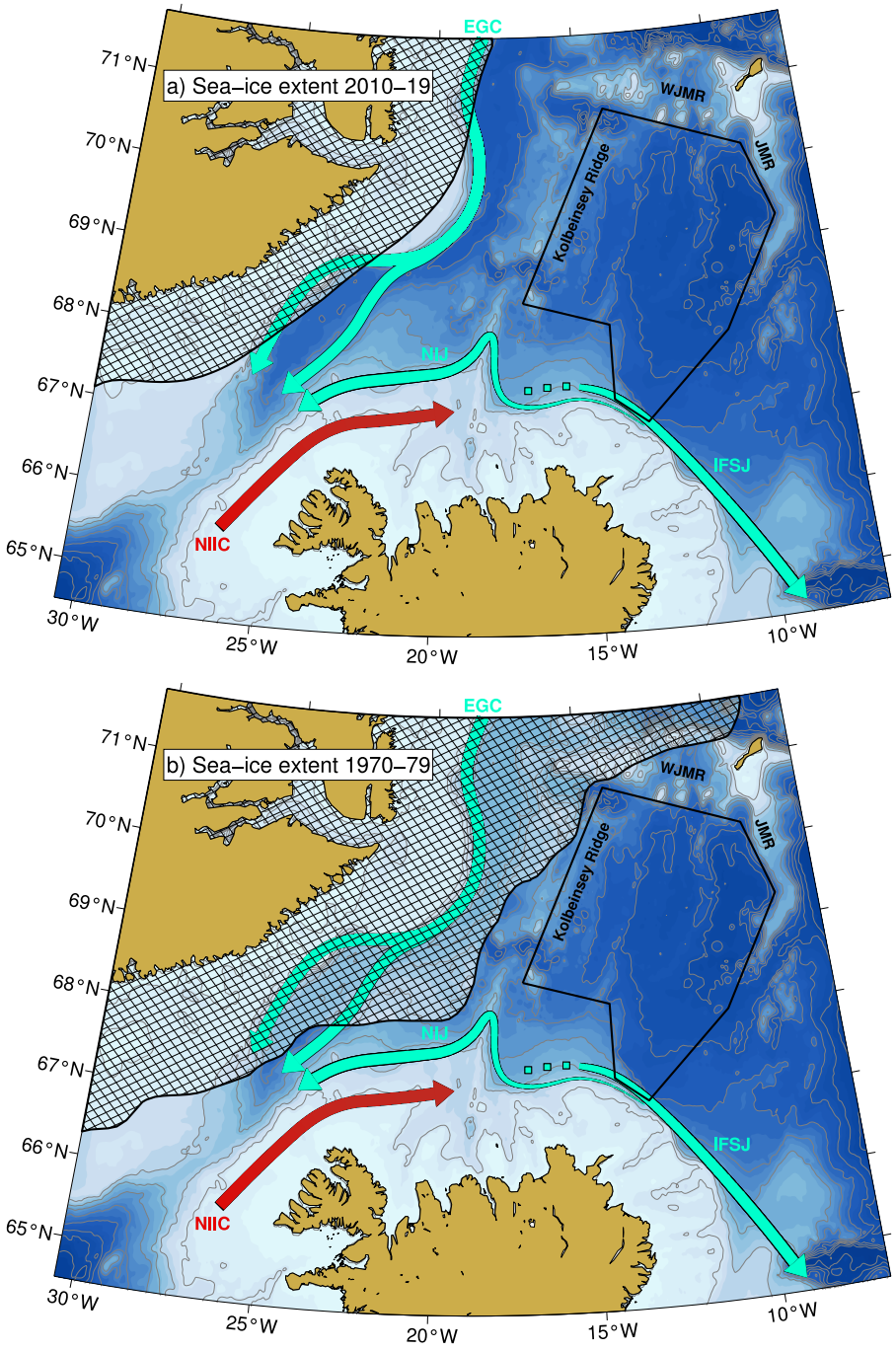


**Fig. 7.** Decadal change in sea-ice extent over the Iceland Sea. The hatched areas represent mean February–April ERA5 sea-ice concentrations in excess of 50% for the periods 2010–19 (a) and 1970–79 (b). The black polygon outlines the control volume from Fig. 1. The dashed portion of the IFSJ indicates its uncertain origin. The acronyms are: EGC = East Greenland Current; NIJ = North Icelandic Jet; IFSJ = Iceland–Faroe Slope Jet; NIIC = North Icelandic Irminger Current; WJMR = West Jan Mayen Ridge; JMR = Jan Mayen Ridge.

## References


Amante, C., Eakins, B.W., 2009. ETOPO1 1 arc-minute global relief model: Procedures, data sources and analysis. Tech. rep., NOAA Technical Memorandum NESDIS NGDC-24, http://dx.doi.org/10.7289/V5C8276M.

Bell, B., Hersbach, H., Simmons, A., Berrisford, P., Dahlgren, P., Horányi, A., Muñoz-Sabater, J., Nicolas, J., Radu, R., Schepers, D., Soci, C., Villaume, S., Bidlot, J.-R., Haimberger, L., Woollen, J., Buontempo, C., Thépaut, J.-N., 2021. The ERA5 global reanalysis: Preliminary extension to 1950. Q. J. R. Meteorol. Soc. 147, 4186–4227. http://dx.doi.org/10.1002/qj.4174.

Brakstad, A., Våge, K., Håvik, L., Moore, G.W.K., 2019. Water mass transformation in the Greenland Sea during the period 1986–2016. J. Phys. Oceanogr. 49, 121–140. http://dx.doi.org/10.1175/JPO-D-17-0273.1.

Chafik, L., Hátún, H., Kjellson, J., Larsen, K.M.H., Rossby, T., Berx, B., 2020. Discovery of an unrecognized pathway carrying overflow waters toward the Faroe Bank Channel. Nature Commun. 11, http://dx.doi.org/10.1038/s41467-020-17426-8.

Chafik, L., Rossby, T., 2019. Volume, heat, and freshwater divergences in the Subpolar North Atlantic suggest the Nordic Seas as key to the state of the Meridional Overturning Circulation. Geophys. Res. Lett. 46, http://dx.doi.org/10.1029/2019GL082110.

Davis, R.E., 1998. Preliminary results from directly measuring middepth circulation in the tropical and south Pacific. J. Geophys. Res. 103, 24619–24639. http://dx.doi.org/10.1029/98JC01913.

de Jong, M.F., Søiland, H., Bower, A.S., Furey, H.H., 2018. The subsurface circulation of the Iceland Sea observed with RAFOS floats. Deep Sea Res. I 141, 1–10. http://dx.doi.org/10.1016/j.dsr.2018.07.008.

Dickson, R.R., Brown, J., 1994. The production of North Atlantic Deep Water: Sources, rates and pathways. J. Geophys. Res. 99, 12319–12341. http://dx.doi.org/10.1029/94JC00530.

Fogelqvist, E., Blindheim, J., Tanhua, T., Østerhus, S., Buch, E., Rey, F., 2003. Greenland-Scotland overflow studied by hydro-chemical multivariate analysis. Deep Sea Res. I 50, 73–102. http://dx.doi.org/10.1016/S0967-0637(02)00131-0.

Harden, B.E., Pickart, R.S., Valdimarsson, H., Richards, C., Våge, K., de Steur, L., Bahr, F., Torres, D.J., Børve, E., Jónsson, S., Macrander, A., Østerhus, S., Håvik, L., Hattermann, T., 2016. Upstream sources of the Denmark Strait overflow: Observations from a high-resolution mooring array. Deep Sea Res. I 112, 94–112. http://dx.doi.org/10.1016/j.dsr.2016.02.007.

Hersbach, H., Bell, B., Berrisford, P., Hirahara, S., Horányi, A., Muñoz-Sabater, J., Nicolas, J., Peubey, C., Radu, R., Schepers, D., Simmons, A., Soci, C., Abdalla, S., Abellan, X., Balsamo, G., Bechtold, P., Biavati, G., Bidlot, J., Bonavita, M., De Chiara, G., Dahlgren, P., Dee, D., Diamantakis, M., Dragani, R., Flemming, J., Forbes, R., Fuentes, M., Geer, A., Haimberger, L., Healy, S., Hogan, R.J., Hólm, E., Janisková, M., Keeley, S., Laloyaux, P., Lopez, P., Lupu, C., Radnoti, G., de Rosnay, P., Rozum, I., Vamborg, F., Villaume, S., Thépaut, J.-N., 2020. The ERA5 global reanalysis. Q. J. R. Meteorol. Soc. 146, 1999–2049. http://dx.doi.org/10.1002/qj.3803.

Huang, J., Pickart, R.S., Bahr, F., McRaven, L.T., Xu, F., 2021. Wintertime water mass transformation in the western Iceland and Greenland Seas. J. Geophys. Res. Oceans 126, http://dx.doi.org/10.1029/2020JC016893.

Huang, J., Pickart, R.S., Huang, R.X., Lin, P., Brakstad, A., Xu, F., 2020. Sources and upstream pathways of the densest overflow in the Nordic Seas. Nature Commun. http://dx.doi.org/10.1038/s41467-020-19050-y.

Jeansson, E., Olsen, A., Jutterström, S., 2017. Arctic Intermediate Water In the Nordic Seas, 1991–2009. Deep Sea Res. I 128, 82–97. http://dx.doi.org/10.1016/j.dsr.2017.08.013.

Jochumsen, K., Moritz, M., Nunes, N., Quadfasel, D., Larsen, K.M.H., Hansen, B., Valdimarsson, H., Jónsson, S., 2017. Revised transport estimates of the Denmark Strait overflow. J. Geophys. Res. Oceans 122, 3434–3450. http://dx.doi.org/10.1002/2017JC012803.

Jónsson, S., Valdimarsson, H., 2004. A new path for the Denmark Strait overflow water from the Iceland Sea to Denmark Strait. Geophys. Res. Lett. 31 (L03305), http://dx.doi.org/10.1029/2003GL019214.

Lauvset, S.K., Brakstad, A., Våge, K., Olsen, A., Jeansson, E., Mork, K.A., 2018. Continued warming, salinification and oxygenation of the Greenland Sea gyre. Tellus A 70, http://dx.doi.org/10.1080/16000870.2018.1476434.

Lozier, M.S., Li, F., Bacon, S., Bahr, F., Bower, A.S., Cunningham, S.A., de Jong, M.F., de Steur, L., de Young, B., Fischer, J., Gary, S.F., Greenan, B.J.W., Holliday, N.P., Houk, A., Houpert, L., Inall, M.E., Johns, W.E., Johnson, H.L., Johnson, C., Karstensen, J., Koman, G., Le Bras, I.A., Lin, X., Mackay, N., Marshall, D.P., Mercier, H., Oltmanns, M., Pickart, R.S., Ramsey, A.L., Rayner, D., Straneo, F., Thierry, V., Torres, D.J., Williams, R.G., Wilson, C., Yang, J., Yashayaev, I., Zhao, J., 2019. A sea change in our view of overturning in the subpolar North Atlantic. Science 363, 516–521. http://dx.doi.org/10.1126/science.aau6592.

Macrander, A., Valdimarsson, H., Jónsson, S., 2014. Improved transport estimate of the East Icelandic Current 2002–2012. J. Geophys. Res. 119, 3407–3424. http://dx.doi.org/10.1002/2013JC009517.

Mastropole, D., Pickart, R.S., Valdimarsson, H., Våge, K., Jochumsen, K., Girton, J., 2017. On the hydrography of Denmark Strait. J. Geophys. Res. Oceans 122, 306–321. http://dx.doi.org/10.1002/2016JC012007.

Mauritzen, C., 1996. Production of dense overflow waters feeding the North Atlantic across the Greenland-Scotland Ridge. Part 1: Evidence for a revised circulation scheme. Deep Sea Res. I 43, 769–806. http://dx.doi.org/10.1016/0967-0637(96)00037-4.

Moore, G.W.K., Våge, K., Pickart, R.S., Renfrew, I.A., 2015. Decreasing intensity of open-ocean convection in the Greenland and Iceland Seas. Nature Clim. Change 5, http://dx.doi.org/10.1038/nclimate2688.

Moore, G.W.K., Våge, K., Renfrew, I.A., Pickart, R.S., 2022. Sea-ice retreat suggests re-organization of water mass transformation in the Nordic and Barents Seas. Nature Commun. 13, http://dx.doi.org/10.1038/s41467-021-27641-6.

Mork, K.A., Skagseth, Ø., Ivshin, V., Ozhigin, V., Hughes, S.L., Valdimarsson, H., 2014. Advective and atmospheric forced changes in heat and fresh water content in the Norwegian Sea, 1951–2010. Geophys. Res. Lett. 41, http://dx.doi.org/10.1002/2014GL061038.

Nøst, O.A., Isachsen, P.E., 2003. The large-scale time-mean ocean circulation in the Nordic Seas and Arctic Ocean estimated from simplified dynamics. J. Mar. Res. 61, 175–210. http://dx.doi.org/10.1357/002224003322005069.

Østerhus, S., Woodgate, R., Valdimarsson, H., Turrell, W.R., de Steur, L., Quadfasel, D., Olsen, S.M., Moritz, M., Lee, C.M., Larsen, K.M.H., Jónsson, S., Johnson, C., Jochumsen, K., Hansen, B., Curry, B., Cunningham, S., Berx, B., 2019. Arctic Mediterranean exchanges: A consistent volume budget and trends in transports from two decades of observations. Ocean Sci. 15, 379–399. http://dx.doi.org/10.5194/os-15-379-2019.

Papritz, L., Spengler, T., 2017. A Lagrangian climatology of wintertime cold air outbreaks in the Irminger and Nordic Seas and their role in shaping air-sea heat fluxes. J. Clim. 30, 2717–2737. http://dx.doi.org/10.1175/JCLI-D-16-0605.1.

Petit, T., Lozier, M.S., Josey, S.A., Cunningham, S.A., 2020. Atlantic deep water formation occurs primarily in the Iceland Basin and Irminger Sea by local buoyancy forcing. Geophys. Res. Lett. 47, http://dx.doi.org/10.1029/2020GL091028.

Pickart, R.S., Moore, G.W.K., Torres, D.J., Våge, K., Valdimarsson, H., Nobre, C., Moore, G.W.K., Jónsson, S., Mastropole, D., 2017. The North Icelandic Jet and its relationship to the North Icelandic Irminger Current. J. Mar. Res. 75, 605–639. http://dx.doi.org/10.1357/002224017822109505.

Pope, J.O., Bracegirdle, T.J., Renfrew, I.A., Elvidge, A.D., 2020. The impact of wintertime sea-ice anomalies on high surface heat flux events in the Iceland and Greenland Seas. Clim. Dynam. 54, 1937–1952. http://dx.doi.org/10.1007/s00382-019-05095-3.

Price, J.F., Weller, R.A., Pinkel, R., 1986. Diurnal cycling: Observations and models of the upper ocean response to diurnal heating, cooling, and wind mixing. J. Geophys. Res. 91, 8411–8427. http://dx.doi.org/10.1029/JC091iC07p08411.

Renfrew, I.A., Barrell, C., Elvidge, A.D., Brooke, J.K., Duscha, C., King, J.C., Kristiansen, J., Lachlan-Cope, T., Moore, G.W.K., Pickart, R.S., Reuder, J., Sandu, I., Sergeev, D., Terpstra, A., Våge, K., Weiss, A., 2021. An evaluation of surface meteorology and fluxes over the Iceland and Greenland Seas in ERA5 reanalysis: The impact of sea ice distribution. Q. J. R. Meteorol. Soc. 147, 691–712. http://dx.doi.org/10.1002/qj.3941.

Renfrew, I.A., Pickart, R.S., Våge, K., Moore, G.W.K., Bracegirdle, T., Elvidge, A.D., Jeansson, E., Lachlan-Cope, T., Papritz, L., Reuder, J., Sodemann, H., Terpstra, A., Waterman, S., Valdimarsson, H., Weiss, A., Almansi, M., Bahr, F., Brakstad, A., Barrell, C., Brooke, J.K., Brooks, B.J., Brooks, I.M., Brooks, M.E., Bruvik, E.M., Duscha, C., Fer, I., Golid, H.M., Hallerstig, M., Hessevik, I., Huang, J., Houghton, L., Jónsson, S., Jonassen, M., Jackson, K., Kvalsund, K., Kolstad, E.W., Konstali, K., Kristiansen, J., Ladkin, R., Lin, P., Macrander, A., Mitchell, A., Olafsson, H., Pacini, A., Payne, C., Palmason, B., Pérez-Hernández, M.D., Peterson, A.K., Petersen, G.N., Pisareva, M.N., Pope, J.O., Seidl, A., Semper, S., Sergeev, D., Skjelsvik, S., Søiland, H., Smith, D., Spall, M.A., Spengler, T., Touzeau, A., Tupper, G., Weng, Y., Williams, K., Yang, X., Zhou, S., 2019. The Iceland Greenland Seas project. Bull. Am. Meteorol. Soc. 100, 1795–1817. http://dx.doi.org/10.1175/BAMS-D-18-0217.1.

Semper, S., Pickart, R.S., Våge, K., Larsen, K.M.H., Hátún, H., Hansen, B., 2020. The Iceland-Faroe Slope Jet: A conduit for dense water toward the Faroe Bank Channel overflow. Nature Commun. 11, http://dx.doi.org/10.1038/s41467-020-19049-5.

Semper, S., Våge, K., Pickart, R.S., Valdimarsson, H., Torres, D.J., Jónsson, S., 2019. The emergence of the North Icelandic Jet and its evolution from northeast Iceland to Denmark Strait. J. Phys. Oceanogr. 49, 2499–2521. http://dx.doi.org/10.1175/JPO-D-19-0088.1.

Smedsrud, L.H., Brakstad, A., Madonna, E., Muilwijk, M., Lauvset, S.K., Spensberger, C., Born, A., Eldevik, T., Drange, H., Jeansson, E., Li, C., Olsen, A., Skagseth, Ø., Slater, D.A., Straneo, F., Våge, K., Årthun, M., 2022. Nordic Seas heat loss, Atlantic inflow, and Arctic sea ice cover over the last century. Rev. Geophys. 60, http://dx.doi.org/10.1029/2020RG000725.

Spall, M.A., Almansi, M., Huang, J., Haine, T.W.N., Pickart, R.S., 2021. Lateral redistribution of heat and salt in the Nordic Seas. Prog. Oceanogr. 196, http://dx.doi.org/10.1016/j.pocean.2021.102609.

Spensberger, C., Spengler, T., 2021. Sensitivity of air-sea heat exchange in cold-air outbreaks to model resolution and sea-ice distribution. J. Geophys. Res.: Atmos. 126, http://dx.doi.org/10.1029/2020JD033610.

Strass, V.H., Fahrbach, E., Schauer, U., Sellmann, L., 1993. Formation of Denmark Strait overflow water by mixing in the East Greenland Current. J. Geophys. Res. 98, 6907–6919. http://dx.doi.org/10.1029/92JC02732.

Swift, J.H., Aagaard, K., 1981. Seasonal transitions and water mass formation in the Iceland and Greenland Seas. Deep Sea Res. 28, 1107–1129. http://dx.doi.org/10.1016/0198-0149(81)90050-9.

Swift, J.H., Aagaard, K., Malmberg, S.-A., 1980. The contribution of the Denmark Strait overflow to the deep North Atlantic. Deep Sea Res. 27A, 29–42. http://dx.doi.org/10.1016/0198-0149(80)90070-9.

Terpstra, A., Renfrew, I.A., Sergeev, D.E., 2021. Characteristics of cold-air outbreak events and associated polar mesoscale cyclogenesis over the North Atlantic region. J. Clim. 34, 4567–4584. http://dx.doi.org/10.1175/JCLI-D-20-0595.1.

Tsubouchi, T., Våge, K., Hansen, B., Larsen, K.M.H., Østerhus, S., Johnson, C., Jónsson, S., Valdimarsson, H., 2021. Increased ocean heat transport into the Nordic Seas and Arctic Ocean over the period 1993–2016. Nature Clim. Change 11, http://dx.doi.org/10.1038/s41558-020-00941-3.

Turrell, W.R., Slesser, G., Adams, R.D., Payne, R., Gillibrand, P.A., 1999. Decadal variability in the composition of Faroe Shetland Channel bottom water. Deep Sea Res. I 46, 1–25. http://dx.doi.org/10.1016/S0967-0637(98)00067-3.

Våge, K., Moore, G.W.K., Valdimarsson, H., Jónsson, S., 2015. Water mass transformation in the Iceland Sea. Deep Sea Res. I 101, 98–109. http://dx.doi.org/10.1016/j.dsr.2015.04.001.

Våge, K., Papritz, L., Håvik, L., Spall, M.A., Moore, G.W.K., 2018. Ocean convection linked to the recent ice edge retreat along east Greenland. Nature Commun. 9, http://dx.doi.org/10.1038/s41467-018-03468-6.

Våge, K., Pickart, R.S., Spall, M.A., Moore, G.W.K., Valdimarsson, H., Torres, D.J., Erofeeva, S.Y., Nilsen, J.E.Ø., 2013. Revised circulation scheme north of the Denmark Strait. Deep Sea Res. I 79, 20–39. http://dx.doi.org/10.1016/j.dsr.2013.05.007.

Våge, K., Pickart, R.S., Spall, M.A., Valdimarsson, H., Jónsson, S., Torres, D.J., Østerhus, S., Eldevik, T., 2011. Significant role of the North Icelandic Jet in the formation of Denmark Strait overflow water. Nat. Geosci. 4, 723–727. http://dx.doi.org/10.1038/NGEO1234.

Wong, A.P.S., Johnson, G.C., Owens, W.B., 2003. Delayed-mode calibration of autonomous CTD float profiling salinity data by $\theta$-S climatology. J. Atmos. Ocean. Technol. 20, 308–318. http://dx.doi.org/10.1175/1520-0426(2003)020<0308:DMCOAC>2.0.CO;2.

Wong, A.P.S., Wijffels, S.E., Riser, S.C., Pouliquen, S., Hosoda, S., Roemmich, D., Gilson, J., Johnson, G.C., Martini, K., Murphy, D.J., Scanderbeg, M., et al., 2020. Argo data 1999–2019: Two million temperature-salinity profiles and subsurface velocity observations from a global array of profiling floats. Front. Mar. Sci. 7, http://dx.doi.org/10.3389/fmars.2020.00700.

Wu, Y., Stevens, D.P., Renfrew, I.A., Zhai, X., 2021. The response of the Nordic Seas to wintertime sea ice retreat. J. Clim. 34, 6041–6056. http://dx.doi.org/10.1175/JCLI-D-20-0932.1.

Yang, J., Pratt, L.J., 2013. On the effective capacity of the dense-water reservoir for the Nordic Seas overflow: Some effects of topography and wind stress. J. Phys. Oceanogr. 43, 418–431. http://dx.doi.org/10.1175/JPO-D-12-087.1.

Yashayaev, I., 2007. Hydrographic changes in the Labrador Sea, 1960–2005. Prog. Oceanogr. 73, 242–276. http://dx.doi.org/10.1016/j.pocean.2007.04.015.